MINES Saint-Étienne

Une école de l'IMT

issia

ECSIA'2021

13th European Congress for Stereology and Image Analysis

28-30 June 2021

Saint-Étienne (France)

https://ecsia2021.sciencesconf.org/

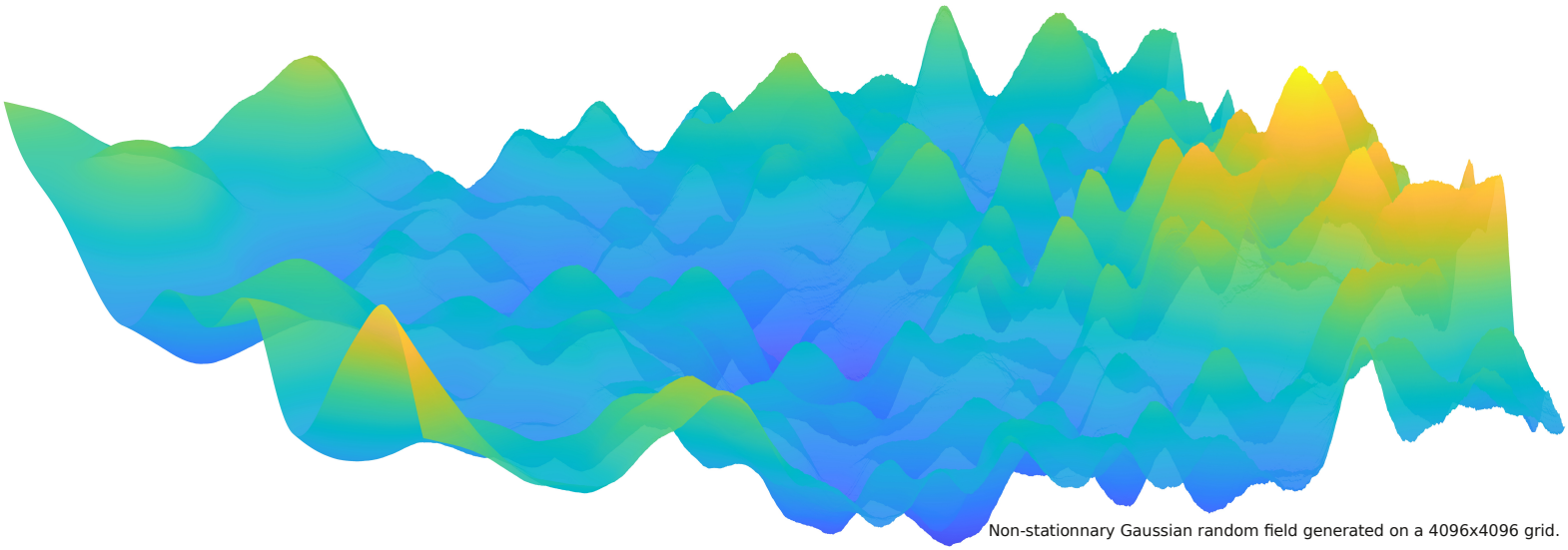

Non-stationnary Gaussian random field generated on a 4096x4096 grid.

Supported by:

LGF UMR 5307 MATERIAUX, MECANIQUE, PROCEDES

GDR GeoSto

cnrs dépasser les frontières

PREFACE

Dear participants of the European Congress on Stereology and Image Analysis,

Let me welcome you online in Saint-Etienne on behalf of the International Society for Stereology and Image Analysis (ISSIA). ECSIA is already the 13th European Congress organized under the auspices of the former International Society for Stereology, now ISSIA. It alternates with International Congress every two years. I am sure that this congress will bring you a lot of new information, inspiration and contacts.

First of all, I would like to invite you to the talk of Mathieu de Langlard, the winner of the PhD Competition in Stereology and Image Analysis, held on Wednesday, 30th June. Mathieu worked on his PhD thesis "Stochastic geometry for 3D characterization of dense particle populations: application to two-phase flows" under the supervision of Prof. Johan Debayle (MINES Saint-Etienne, France), Sophie Charton and Fabrice Lamadie (CEA Marcoule, France). Please, do not miss this opportunity. I would like to thank all the applicants as well as the members of the evaluation committee who carefully evaluated all submitted theses and found them to be of very high quality.

Furthermore, I would like to invite all ISSIA members to the General Assembly, which will be held at 17:15 on Tuesday, 29th June. For those who are not ISSIA members yet – please consider becoming a member – you are very much welcome to come to the meeting as well, so that you can learn more about our Society. In brief, the International Society for Stereology and Image Analysis (www.issia.net) is an international scientific society that aims to promote stereology and image analysis in a wide range of disciplines, such as mathematics, biomedicine, physics, geology, metallurgy, plant biology, etc. The official journal of ISSIA is Image Analysis & Stereology (www.ias-iss.org). ISSIA members are eligible for reduced publication fees in the open-access IAS journal. Other benefits of ISSIA membership include reduced rates at congresses, courses and workshops organized by ISSIA; possibility for student members to apply for Hans Elias bursaries enabling participation in ISSIA Congresses; possibility to take part in a competition for the best PhD thesis using stereology and/or image analysis, and access to the LinkedIn forum (www.linkedin.com/groups/4239739).

Last but not least, I would like to express my gratitude and appreciation to the ECSIA organizers, especially Johan Debayle and Yann Gavet, for their tremendous efforts in organizing this event.

Wishing you a pleasant and fruitful time during the congress,

Ales Kladnik
ISSIA President

ECSIA'2021 Conference Program

June 28-30, 2021
Saint-Etienne, France

CET time	Monday, June 28	
9h00 – 9h30	Opening / Welcome	
9h30 – 10h25	**Keynote 1: Image analysis and machine learning applied to fighting against cybercrime** Prof. Enrique Alegre *Group for Vision and Intelligent Systems (GVIS), University of León, Spain* Chair: Beatriz Marcotegui	
10h25 – 10h40	Break time	
10h40 – 11h55	**Session 1: Mathematical Morphology (MM)** Chair: Jens Randel Nyengaard	
	10h40	**3D adaptive morphology applied to fiber orientation analysis** Barisin Tin (1) (2), Schladitz Katja (1), Godehardt Michael (1), Redenbach Claudia (2) *1 - Fraunhofer Institute of Industrial Mathematics (Kaiserslautern, Germany)* *2 - Fachbereich Mathematik (Kaiserslaiteurn, Germany)*
	11h05	**Analysis of wheat grains growth using improved 3D morphological filtering** Legland David (1), Le Thang Duong Quoc (2), Chateigner-Boutin Anne-Laure (2), Girousse Christine (3) *1 - Unité de recherche sur les Biopolymères Interactions Assemblages (Angers/Nantes France)* *2 - UR 1268 BIA (Nantes, France)* *3 - UMR INRAE/UCA, Génétique Diversité et Ecophysiologie des Céréales (Clermont-Ferrand, France)*
	11h30	**Water-skel** Marcotegui Beatriz (1), Decencière Etienne (1), Borocco Albane (1) *1 - MINES Paris-Tech, Centre de Morphologie Mathématique (Fontainebleau, France)*
11h55 – 14h00	Lunch time / **ISSIA Board Meeting**	
14h00 – 15h30	**Mini-Course: Part 1/2** Chair: Daniel Peterson	
	14h00	**Mathematical morphology meets Deep Learning** Velasco-Forero Santiago (1), Blusseau Samy (1), Sangalli Mateus (1) *1 - MINES ParisTech, Centre de Morphologie Mathématique (Fontainebleau, France)*
15h30 – 15h45	Break time	
15h45 – 17h15	**Mini-Course: Part 2/2** Chair: Daniel Peterson	
	15h45	**Mathematical morphology meets Deep Learning** Velasco-Forero Santiago (1), Blusseau Samy (1), Sangalli Mateus (1) *1 - MINES ParisTech, Centre de Morphologie Mathématique (Fontainebleau, France)*

CET time	Tuesday, June 29	
9h00 – 9h55	**Keynote 2: Towards Development of an Intelligent System for Thyroid Cancer Detection** Ass. Prof. Hanung Adi Nugroho *Department of Electrical and Information Engineering, Faculty of Engineering, Universitas Gadjah Mada, Yogyakarta, Indonesia* Chair: Ida Erzen	
9h55 – 10h45	**Session 2: Image Processing and Analysis (IPA)** Chair: Bruno Figliuzzi	
	9h55	**Vector fields color constancy correction within the CoLIP framework** Crozier Thomas (1), Gavet Yann (1) *1 - MINES Saint-Etienne (Saint-Etienne, France)*
	10h20	**Mass Fractal Dimension estimate from Microscopy Images using Morphological Aggregation Model** Ferri Giulia (1), Humbert Severine (1), Digne Mathieu (1), Schweitzer Jean-Marc (1), Moreaud Maxime (1) (2) *1 - IFP Energies Nouvelles (Solaize, France)* *2 - MINES ParisTech, PSL-Research University, CMM (Fontainebleau, France)*
10h45 – 11h00	Break time	
11h00 – 12h15	**Session 3: Image Processing and Analysis (IPA)** Chair: Ales Kladnik	
	11h00	**Particles detection in a 2D-image of overlapping crystals based on community detection** Rahmani Said (1), De Souza Lima Roger (1), Cameirão Ana (1), Serris Eric (1), Debayle Johan (1) *1 - MINES Saint-Etienne (Saint-Etienne, France)*
	11h25	**Performance of Digital Image Enhancement Algorithm for Plasmodium Parasite Detection using Thick Blood Smear Digital Microscopic Images** Nugroho Hanung Adi (1), Nurfauzi Rizki (1), Frannita Eka Legya (1) *1 - Universitas Gadjah Mada (Yogyakarta, Indonesia)*
	11h50	**M-tortuosity formalism; from binary to structural and functional characterization** Chaniot Johan (1), Moreaud Maxime (2), Sorbier Loïc (3), Lévesque Sébastien A. (1), Bélanger Erik (1), Becker Jean-Marie (4), Fournel Thierry (4), Jeulin Dominique (5), Marquet Pierre (1) *1 - Centre de recherche CERVO (Canada)* *2 - IFP Energies Nouvelles / MINES ParisTech (Paris, France)* *3 - IFP Energies Nouvelles (Solaize, France)* *4 - Laboratoire Hubert Curien (Saint-Etienne, France)* *5 - MINES ParisTech, Centre de Morphologie Mathématique (Fontainebleau, France)*
12h15 – 14h00	Lunch time	
14h00 – 14h55	**Keynote 3: Parallel sets in density estimation: theoretical results with a glance at possible applications and further developments** Ass. Prof. Elena Villa *Dept. of Mathematics, Università degli Studi di Milano, Italy* Chair: Viktor Benes	
14h55 – 15h45	**Session 4: Stochastic Geometry, Statistics (SGS)** Chair: Maxime Moreaud	
	14h55	**Birth and death simulation of human corneal endothelium cells** Thuret Gilles (1), He Zhiguo (1), Vaitinadapoulle Hanielle (1), El Amri Hatem (1), Ben Moussa Olfa (1), Thomas Justin (1), Mascarelli Frederic (1), Gain Philippe (1), Gavet Yann (2) *1 - Biologie, Ingénierie et Imagerie de la Greffe de Cornée (Saint-Etienne, France)* *2 - MINES Saint-Etienne (Saint-Etienne, France)*
	15h20	**Estimation of summary characteristics for random closed sets** Pawlas Zbyněk (1) *1 - Charles University (Prague, Czech Republic)*
15h45 – 16h00	Break time	

16h00 – 17h15	**Session 5: Stochastic Geometry, Statistics (SGS)** Chair: Dominique Jeulin	
	16h00	**Morphological models characterization: a Bayesian approach** Figliuzzi Bruno (1) *1 – MINES ParisTech, Centre de Morphologie Mathématique (Fontainebleau, France)*
	16h25	**Random tessellations marked with crystallographic orientations** Karafiátová Iva (1), Pawlas Zbyněk (1), Heller Luděk (2) *1 - Charles University (Prague, Czech Republic)* *2 - Czech Academy of Sciences (Prague, Czech Republic)*
	16h50	**Sensitivity of the local measures to deviations of the typical grain shape in Boolean models** Eremina Tatyana (1), Debayle Johan (1), Gruy Frédéric (1), Pinoli Jean-Charles (1) *1 - MINES Saint-Etienne (Saint-Etienne, France)*
17h15 – 18h15	ISSIA General Assembly	

CET time	Wednesday, June 30	
9h00 – 9h55	**Keynote 4: First Commercial Dual MeV Energy X-ray CT for Container Inspection: System, Algorithm and Results** Ass. Prof. Liang Li *Department of Engineering Physics, Tsinghua University, Beijing, China* Chair: Katja Schladitz	
9h55 – 10h25	**ISSIA Best PhD Thesis** Chair: Bruno Figliuzzi	
	9h55	**Stochastic geometry for 3D characterization of dense particle populations: application to two-phase flows** de Langlard Mathieu (1) (2) *1 - MINES Saint-Etienne (Saint-Etienne, France)* *2 - CEA (Marcoule, France)*
10h25 – 10h40	Break time	
10h40 – 11h55	**Session 6: Applications (APP)** Chair: Dorothy Oorschot	
	10h40	**Comparison of segmentation of 2D and 3D EBSD measurements in polycrystalline materials** Stanek Jakub (1), Kopecek Jaromir (2), Kral Petr (3), Karafiátová Iva (1), Seitl Filip (1), Benes Viktor (1) *1 - Faculty of Mathematics and Physics, Charles University (Prague, Czech Republic)* *2 - Institute of Physics CAS (Prague, Czech Republic)* *3 - Institute of Physics of Materials CAS (Prague, Czech Republic)*
	11h05	**Lycopene increases the number of osteocytes in the femur of female rats with osteoporosis** Coppi Augusto (1), Semeghini Mayara (2), Siessere Selma (2), Bombonato-Prado Karina (2) *1 - Nottingham Trent University (Nottingham, United Kingdom)* *2 - University of São Paulo (São Paulo, Brazil)*
	11h30	**Stochastic models for polycrystalline materials** Seitl Filip (1) *1 - Department of Probability and Mathematical Statistics, Charles University (Prague, Czech Republic)*
11h55 – 14h00	Lunch time	
14h00 – 15h40	**Session 7: Applications (APP)** Chair: David Legland	
	14h00	**Oxide characterization using sparse unmixing** Zenati Tarek (1) (2), Figliuzzi Bruno (1), Ham Grace Shu-Hui (2) *1 - MINES ParisTech, Centre de Morphologie Mathématique (Fontainebleau, France)* *2 - ArcelorMittal Maizières Research SA (Maizières-lès-Metz, France)*
	14h25	**The effects of diabetes type 2 on capillary network of inspiratory muscles analysed by a 3D method** Tit Tomazin Rok (1), Cvetko Erika (1), Alibegović Armin (2), Janáček Jiří (3), Umek Nejc (1) *1 - Institute of Anatomy, Faculty of Medicine, University of Ljubljana (Ljubljana, Slovenia)* *2 - Institute of Forensic Medicine, Faculty of Medicine, University of Ljubljana (Ljubljana Slovenia)* *3 - Department of Biomathematics, Institute of Physiology, Czech Academy of Science (Prague, Czech Republic)*
	14h50	**Stereology of Liver after Sucralose ingestion: Effect and possible hypothesis** Dhurandhar Diwakar (1) *1 - Pt. J.N.M Medical College, Raipur (Chhattisgarh, India)*
	15h15	**Characterization of Pyramidal Cells in Layer III of Brodmann Area 46 in Schizophrenia and Depression** Nick Y. Larsen (1),Jens Randel Nyengaard (1) *1 – Aarhus University, (Aarhus, Denmark)*
15h15 – 15h30	Closing	

Contents

3D adaptive morphology applied to fiber orientation analysis

Tin Barisin[1,2], Michael Godehardt[1], Katja Schladitz[1], Claudia Redenbach[2]

[1]Image Processing Department, Fraunhofer ITWM, Fraunhofer-Platz 1, 67663 Kaiserslautern, Germany,

[2]Department of Mathematics, University of Kaiserslautern 67653 Kaiserslautern, Germany

Email: tin.barisin@itwm.fraunhofer.de, michael.godehardt@itwm.fraunhofer.de, katja.schladitz@itwm.fraunhofer.de, redenbach@mathematik.uni-kl.de

Abstract

Lower dimensional and directed structures like cracks, fibers or closed facets in foams are of particular interest in various applications. Characterization of these structures based on 3D image data is often tied to their local orientation which is in turn used for structure enhancement, directional filtering, segmentation or separation of interacting structures. The idea of using banks of directed structuring elements or filters parameterized by a discrete subset of the orientation space has been around for a while and is proven to be effective for these tasks in 2D (Freeman and Adelson [1], Schladitz et al. [2]).

However, this class of methods is prohibitive in 3D due to high computational burden of a sufficiently fine discretization of the unit sphere (Wirjadi et al. [3]). Many of these structures are not only thin and highly-anisotropic but have additionally a complex shape. Thus the orientation of the structuring element has to fit well in order to achieve good quality results. With our method, we aim at a practicable trade-off between locally fine sensing and computational effort for the 3D case.

We introduce a method for 3D pixel-wise orientation estimation and directional filtering inspired by the idea of adaptive refinement in discretized settings. Our method requires initial estimation of the orientation in each pixel. It subsequently checks the cone around this initial orientation for possible improvements in orientation estimation based on the filter response from the directed structuring element i.e. line or sheet. As a result, our method is able to balance between computational load and robustness of estimation. Two strategies for estimating the initial directions are proposed and discussed.

Finally, we apply our method to the micro-computed tomography image of an injection molded glass fiber reinforced composite sample. It features high fiber volume fraction and long fibers and thus a misoriented region occurs (Figure 1). Since single fiber segmentation is not possible, we have to rely on the local pixel orientation estimation for the investigation of material structure (Wirjadi et al. [4]). Our method provides consistent results for that purpose. We segment fiber bundles (similarly oriented structures in the image) as suggested by Sliseris et al. [5]. Finally, our refinement of the orientation estimation yields a precise segmentation of the misoriented region (Figure 2).

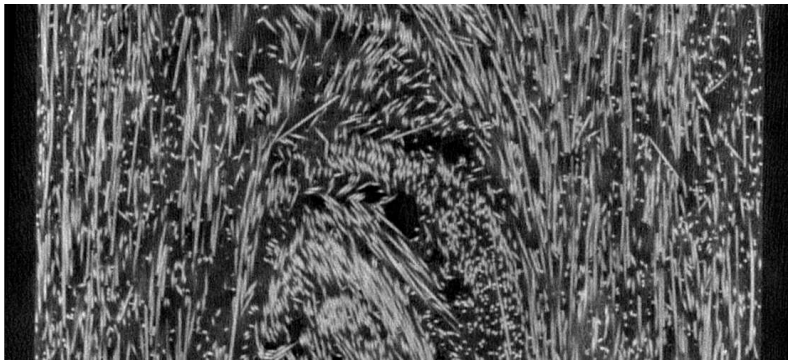

Figure 1: Slice from high volume fiber sample with misaligned region.

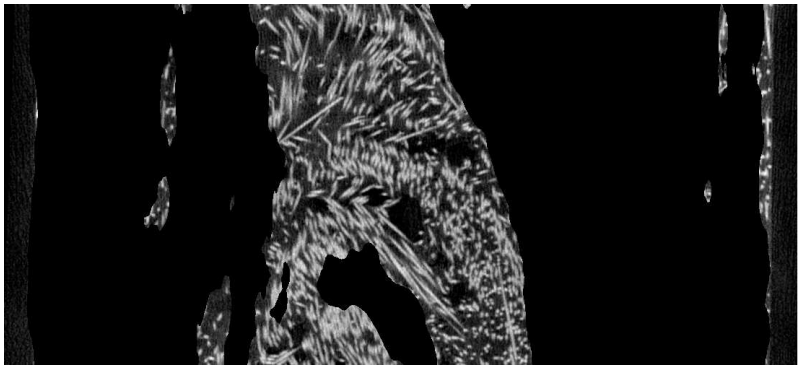

Figure 2: Segmentation of misaligned region.

References

1. W. T. Freeman, W.T. and Adelson, E. H. (1991.). The design and use of steerable filters, IEEE Transactions on Pattern Analysis and Machine Intelligence, vol. 13, no. 9, pp. 891-906,
https://doi.org/10.1109/34.93808

2. Schladitz, K., Büter, A., Godehardt, M., et al. (2017.). Non-destructive characterization of fiber orientation in reinforced SMC as input for simulation based design. Composite Structures, Volume 160, Pages 195-203, ISSN 0263-8223,
https://doi.org/10.1016/j.compstruct.2016.10.019.

3. Wirjadi, O., Schladitz, K., et al., (2016). Estimating Fibre Direction Distributions of Reinforced Composites from Tomographic Images. Image Analysis Stereology, 35(3), 167-179.
https://doi.org/10.5566/ias.1489

4. Wirjadi, O., Godehardt, M., Schladitz, K. et al. (2014). Characterization of multilayer structures of fiber reinforced polymer employing synchrotron and laboratory X-ray CT. International Journal of Materials Research (formerly Zeitschrift fuer Metallkunde). 105. 645–654.
https://doi.org/10.3139/146.111082

5. Sliseris, J., Andrä, H., Kabel, M. et al. (2016). Estimation of fiber orientation and fiber bundles of MDF. Materials and Structures 49, 4003–4012
https://doi.org/10.1617/s11527-015-0769-1

Analysis of wheat grains growth using improved 3D morphological filtering

David Legland[1], Thang D. Q. Le[1], Anne-Laure Chateigner-Boutin[1], Christine Girousse[2]

[1]UR1268 BIA, BIBS, INRAE, 44300 Nantes, France.

[2]UMR GDEC, INRAE, Université Clermont-Auvergne, 63000 Clermont-Ferrand, France

Email: david.legland@inrae.fr

Abstract

Wheat is one of the most important staple source in the world for human and animal consumption. A better understanding of the phenomenons involved in its growth could help improving crop yields, and selecting varieties adapted to climate change.
Grains at various stages of development were imaged by 3D micro-computed tomography, allowing to generate 3D images of individual grain with a voxel size ranging from 4 to 10 microns. An image-processing workflow was developped to quantify the 3D morphology of wheat grains [1]. The workflow comprised segmentation of the grain by multi-class thresholding, re-alignement of the 3D images, identification of tissues within the grain, and quantification of 3D morphometric features (Fig. 1).

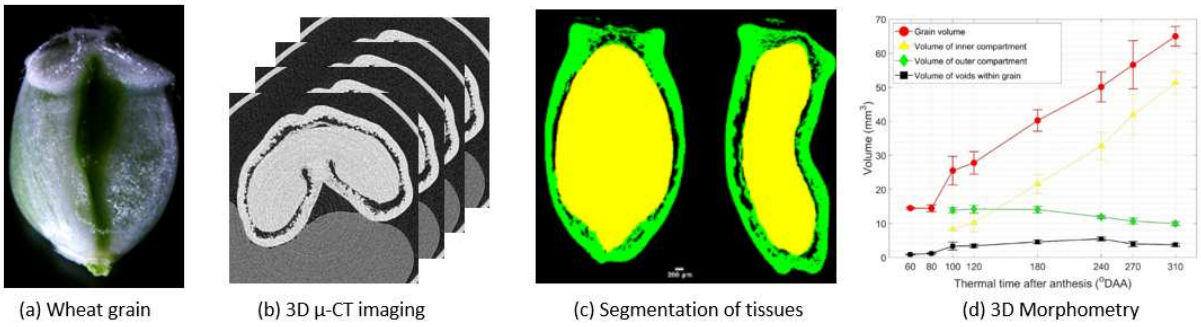

Figure 1: Several steps of the image processing workflow.

The segmentation of the tissues involved morphological filtering on 3D images with large stucturing elements, resulting in large computation times [2]. Using cube-shape structuring elements reduces computational complexity, but introduces artifacts that are not desirable for the analysis of biological organs. An enhanced algorithm was implemented to reduce the computational complexity of morphological operations using spherical structuring elements, based on [3]. The principle consists in considering the local histogram of the values within the structuring element, and to update the histogram based only on the values of the boundary pixels. The resulting complexity decreases from $\mathcal{O}(r^d)$ to $\mathcal{O}(r^{d-1})$, where r is the radius of the structuring element, resulting in faster computations for large structuring elements. Further work about the methodology concern the application of the algorithm to floating-point encoded images.
The application of morphological filters allowed to finely discriminate between inner tissues and outer tissues from 3D images, and to quantify the evolution of their volume over time. More precise quantification of the changes of morphology are currently investigated using shape registration algorithms.

References

1. T. D. Q. Le, C. Alvarado, C. Girousse, D. Legland, A.-L. Chateigner-Boutin. Use of X-ray micro computed tomography imaging to analyze the morphology of wheat grain through its development. *Plant Methods* **15** (1), 84, 2008.

2. P. Soille. *Morphological Image Analysis.* Springer, 2002.

3. M. VanDroogenbroeck and H. Talbot. Fast computation of morphological operations with arbitrary structuring elements. Pattern Recognition Letters 17(14). 1451–1460, 1996.

Water-skel

Beatriz Marcotegui, Etienne Decencière, Albane Borocco

MINES ParisTech, PSL Research University,
35 rue Saint Honoré - Fontainebleau, France
http://cmm.mines-paristech.fr

Email: {beatriz.marcotegui, etienne.decenciere, albane.borocco}@mines-paristech.fr

Abstract

This paper introduces a distance-based skeleton approach. It starts from a set of preselected shape extremities. The extremities lead to the definition of markers on the object boundary. These markers are then immersed on the inverse distance function. Finaly a watershed provides a thin, homotopic and centered skeleton linking the provided extremities. The main contribution of the paper is the interpretation of the skeleton as a watershed process from markers, a well known operator and for which efficient implementations exist.
As extremities detector we use h-maxima of the geodesic distance from the furthest point p of the object to its barycentre. Any other technique could have been used.
Let X be a connected finite subset of $\mathbb{Z}^2$ equipped with a neighborhood relation among $V4$, $V6$ or $V8$ (we generally use $V6$). The process is summarized in the following figure:

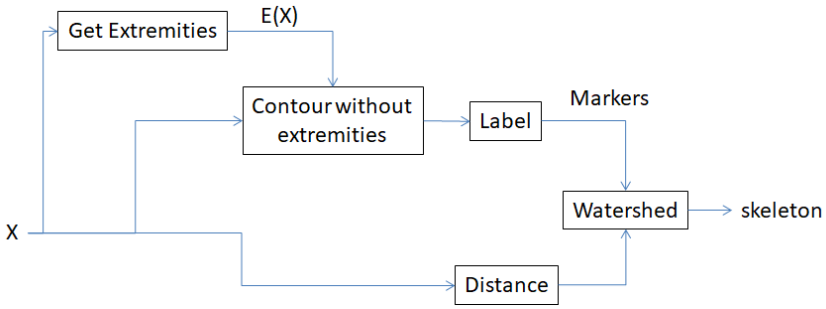

Figure 1: Water-skel flow chart.

Once the extremities have been detected, they can be used as separations between starting fires from the boundary (using Blum's analogy [1]). Considering these boundary portions as markers, combined with the watershed transform of the distance function, the skeleton is found in a single computation. Compared to [3], we focus on extremities to be linked instead of maximall ball centers. Compared to [2] a single watershed process handles all extremities at once.
Fig. 2 illustrates the principle of the method with intermediate images in three different configurations. Fig. 2 (a) illustrates the fact that the method correctly handles holes. Fig. 2 (b) illustrates the main drawback of the method: if there is a single extremity along a connected component of the contour, then the corresponding branch will be absent from the skeleton. If additional extremities are present along the connected component of the contour (see figure 2 (c)) the problem disappears. More generally, if a given extremity E_i cannot reach another extremity E_j with $j \neq i$ following the boundary of the shape (E_i is said to be an isolated extremity), our method misses the branch corresponding to E_i. If this situation appears, an alert can be raised because the corresponding extremity has a

single marker in its neighborhood. The missing branch could be added to the skeleton, following the shortest path as proposed by [2]. Connected components with one or none extremity can be properly managed: correctly handled by the proposed algorithm if the connected component has hole(s), the D thinning skeleton otherwise. We have not run into these situations in our practical usage of the method with real images. This technique has been used successfully in an image registration process of an industrial project [4].

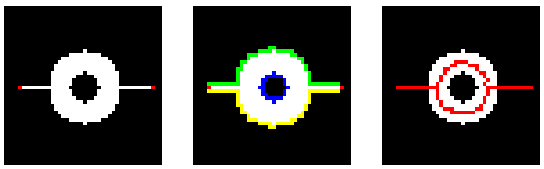

(a) Holes are correctly treated by the proposed method.

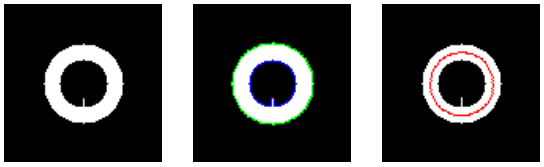

(b) Problem with an isolated extremity.

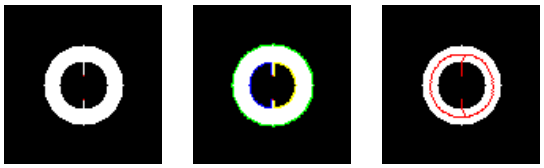

(c) Two extremities in a hole: correct result.

Figure 2: Particular configurations. 1^{st} column: input images and selected extremities (in red). 2^{nd} column: markers. 3^{rd} column: resulting skeleton. Each extremity needs two different labels in its neighborhood. Otherwise, the corresponding branch is missing in the skeleton.

References

1. Harry Blum et al. A transformation for extracting new descriptors of shape, volume 4. MIT press Cambridge, 1967.

2. G Fricout, D Jeulin, L Cullen-Mc Ewen, IS Harper, and JF Bertram. 3D skeletonization of ureteric trees in developing kidneys. Mathematical Morphology VI, Proc. ISMM02, pages 135-157, 2002.

3. Leborgne, A., Mille, J., Tougne, L. Noise-resistant digital euclidean connected skeleton for graph-based shape matching. Journal of Visual Communication and Image Representation, 31, 165-176, 2015.

4. A. Borocco. "Automatisation de la segmentation d'épures constats par des techniques de recalage non rigide et de segmentation sous contraintes". confidential MINES ParisTech PhD defended on February 27th 2020 (public on December 31, 2024).

Vector fields color constancy correction within the CoLIP framework

Thomas Crozier[1], Yann Gavet[1]

[1]Mines Saint-Etienne, Univ. Lyon, CNRS, UMR 5307 LGF, Centre SPIN, F - 42023 Saint-Etienne, France.

Email: gavet@emse.fr

Abstract

Color constancy is the phenomenon that allows human vision to perceive the right color of an object or of a scene despite the scene is enlighted by a non neutral illuminant that leads to a biased reflection of the light on the object. The stake of White Balance Correction is to make an estimation of the scene illuminant and to correct the image. This illuminant is generally estimated with referenced grey objects placed on the scene, the measured chromaticity of these objects is then considered as the chromaticity of the global illuminant of the scene. This method gives a consistent neutral chromaticity on grey objects but may not give the desired result on colored objects.
In this work, a method is proposed to tackle Color Constancy problems within the CoLIP framework. Since we use a dataset having McBetch ColorChecker on each image, with patches of standardized values (18 colored patches and 6 neutral ones going from white to black), we propose a method to adjust the entire image chromaticity so that in the resulting image all the patches correspond to their theoretical values. The 24 patches present on the chart are not enough to correct the whole image, we thus use an interpolation to compute the correction of each pixel. The resulting interpolation gives us a vector field.
These transformations are performed in the CoLIP colorspace [1,2], that has been designed to be physically consistent with the laws of human visual perception. This color space has three channels, an achromatic one and two chromatic ones. Since this color space has not been used in many color constancy tasks, we considered it was necessary to show it can be used for this task. To do so, we applied classic White Balance algorithms such as the White Patch and the Grey World one [3], to show the CoLIP colorspace can provide consistent results.

References

1. M. Jourlin and J.-C. Pinoli. *Logarithmic Image Processing.* Acta Stereologica **6**, 651–656, 1987.

2. Y. Gavet, J. Debayle and J.-C. Pinoli. *The Color Logarithmic Image Processing (CoLIP) Antagonist Space and Chromaticity Diagram* in *Color Image and Video Enhancement* Springer, 155–182, 2015.

3. E. Y. Lam, *Combining gray world and retinex theory for automatic white balance in digital photography* in *Proceedings of the Ninth International Symposium on Consumer Electronics, ISCE*, 2005, pp. 134-139, doi: 10.1109/ISCE.2005.1502356.

Mass Fractal Dimension estimate from Microscopy Images using Morphological Aggregation Model

Giulia Ferri[1], Severine Humbert[1], Mathieu Digne[1], Jean-Marc Schweitzer[1], Maxime Moreaud[1,2]

[1]IFP Energies Nouvelles, RondPoint de l'Echangeur de Solaize, 69360 Solaize.,[2]MINES ParisTech, PSL-Research University, CMM, Fontainebleau, France.

Email: giulia.ferri@ifpen.fr, severine.humbert@ifpen.fr, mathieu.digne@ifepn.fr, jean-marc.schweitzer@ifpen.fr, maxime.moreaud@ifpen.fr

Abstract

The manufacturing process of a γ-alumina catalytic support involves the assembly of boehmite aggregates and agglomerates in an aqueous environment to form complex structures. The operating conditions influence the formation of the solid and the textural properties of the final product [1]. These can be guided by a numerical model of solid microstructure that mimics the properties of the raw material as a function of the physical-chemical parameters of the synthesis.

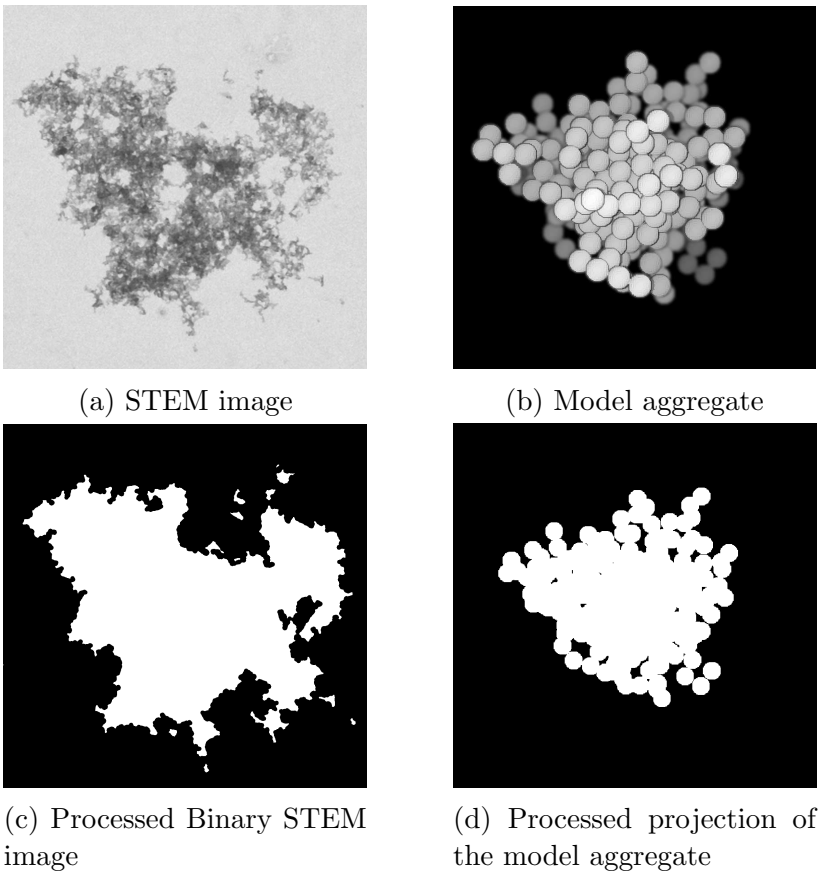

(a) STEM image

(b) Model aggregate

(c) Processed Binary STEM image

(d) Processed projection of the model aggregate

Figure 1: On the left, initial and processed STEM image. On the right, an aggregate generated with the morphological model and its opaque projection.

Mass fractal dimension d_f^{mass} is a key descriptor to characterize the structure of aggregates

and agglomerates. It describes the number of elementary objects (N) in an assembly [2]:

$$N = \left(\frac{R_{gyr}}{a}\right)^{d_f^{mass}}$$

with R_{gyr} the gyration radius and a the particle radius. d_f^{mass} ranges between 1 (for linear structures) and 3 (for spherical structures). Our objective is to estimate d_f^{mass} from STEM images (Fig.1(a)) to feed a model of the solid structure. Our approach follows the one of Liu *et al.* [3] that was applied in another context.

On the one hand, STEM image processing to obtain a binary image (Fig.1(c)) allows the measurement of shape factors of aggregates and agglomerates [4]. Alternatively, the morphological aggregation model from [5] produces 3D clusters with controlled d_f^{mass} (Fig.1(b)). Shape factor measurements are performed on opaque projections of these clusters. The comparison of the shape factors obtained from the STEM images and the opaque projections of the model provides an estimate of d_f^{mass}. To validate our approach, the estimates are compared to those obtained indirectly by Dynamic Light Scattering and Small Angle X-ray Scattering.

References

1. Yang Y. et al. *Journal of Colloid and Interface Science* 2016, 469, 1-7;
2. Filippov A.V. et al. *Journal of Colloid and Interface Science* 2000, 229, 261-273;
3. Moreaud M. et al. *Journal of Microscopy* 2012, 245(2), 186-99;
4. Liu C. et al. *Applied Clay Science* 2011, 54, 97-106;
5. Ferri G. et al. *Journal IAS*, submitted manuscript;

Particles detection in a 2D-image of overlapping crystals based on community detection

Said Rahmani[1], Roger de Souza Lima[1], Ana Cameirão[1], Eric Serris[1], Johan Debayle[1]

[1] MINES Saint Etienne, SPIN/LGF UMR 5307

Email: said.rahmani@emse.fr, roger.de-souza-lima@emse.fr, cameirao@emse.fr, serris@emse.fr, debayle@emse.fr

Abstract

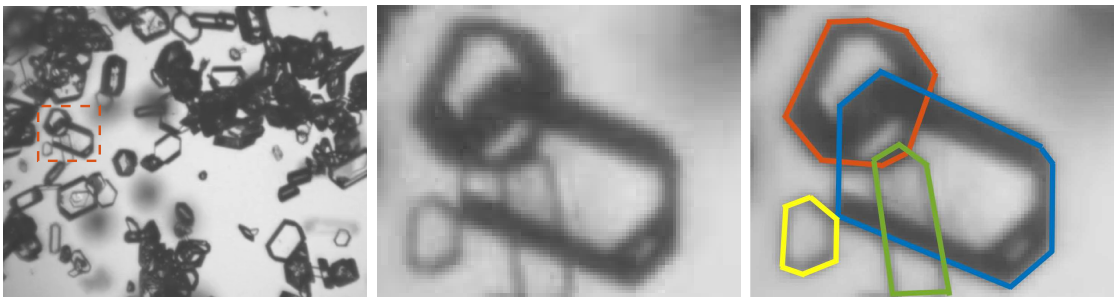

(a) Example of an image (b) A cropped aggregate (c) Identified crystals

Figure 1: An image of Adipic acid crystals and the cropping windows (a), a crop of an aggregate of crystals (b) and its hand made individualization (c).

This work is motivated by the control of industrial crystallisation processes, which involve the knowledge of the crystals distribution over time. For this purpose, an in situ camera in batch crystallisers provide 2D images of the projected crystals population in real time such as Figure 1 (a).In order to characterize the geometry of the overlapped crystals, advanced image processing [1, 2] or stochastic geometry [3] can be used.
The proposed approach in this study is based on community detection (as done in social networks [4]). One can see on the images that the borders of individual crystals is quite visible and such a data Figure 1(b) looks like a tessellation of the union of crystals. Indeed, for instance in Figure 1 (b-c), four polygonal crystals are recognizable from a human visual perception (Gestalt theory [5]). It involves the use of topological and geometrical relationship between tessellation cells to make the decision to put the cells in the same crystal or not. Our objective is to provide an automatic detection of the crystals based on such "community membership" rules.

Formally, one consider a 2D random aggregate A defined as a union of a familly $\mathcal{F}$ of 2D convex sets $\mathcal{F} = \{X_1, \cdots X_n\}$ centred on random position $x := (x_i)_{1 \leq i \leq n}$ as $A = \bigcup_{i=1}^{n} x_i + X_i$ and assume that the random vector of position x has a probability density (this technical condition will be discussed later).
Let $T = \{S_1, \cdots S_N\}$ a tessellation of A which is thinner than the minimal tessellation showing the borders of the convex sets X_i (defined as the tessellation of the aggregate A engendered by the X_i with the intersection and the set difference operators). For such a tessellation T, for any X_i there is a subset of T which is a tessellation of X_i, i.e. for any X_i there is $T_i \subset T$ such that $X_i = \bigcup_{S_j \in T_i} S_j$ (Figure 2 (a)).
We try to get the reconstruction of the full family $\mathcal{F} = \{X_1, \cdots X_n\}$ from the available information on the cells S_k of the tessellation T. Obviously for a given aggregate A and its

tessellation T there is several candidates for the family $\mathcal{F}$. However some considerations allows us to almost surely uniquely define the reconstruction, considering the randomness of A (the fact that x has a density) and the knowledge of the weights of the cells defined as $w(S_i) = \#\{X_k \mid S_i \in T_k\}$.
The geometrical combinatorial problem presented above can be modeled by a graph (Figure 2) and reformulated as a community detection problem, as done in social networks [4]. Indeed, considering that the tessellation cells are the vertices of the graph provided by topological and geometrical relationship on its edges, the convex sets X_i can be seen as communities to find.
We propose an algorithm of detection based on maximal clique detection on our graph provided by the edge relation $\mathcal{R}$ defined as $S_i \mathcal{R} S_j \Leftrightarrow ConvHull(S_i \cup S_j) \subset A$. Notice that for this relation a particle X_i is always a clique (complete subgraph) of the graph (Figure 2 (b)), which is always included in a maximal clique of the graph. The use of such a property (and the particle convexity) with the weights information allows us to identify the particles X_i from the cliques using an iterative algorithm.

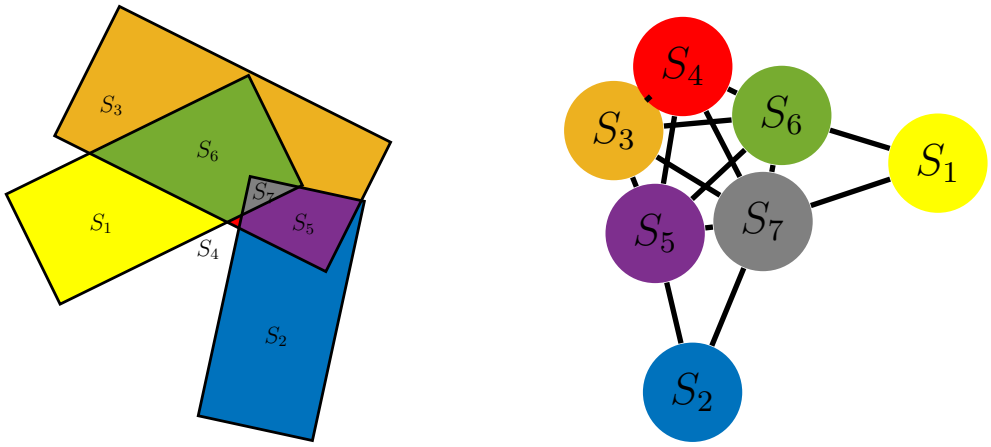

(a) (b)

Figure 2: An aggregate of three rectangle and its minimal tessellation (a). The corresponding graph provided by the convex hull relationship on its edges $\mathcal{R}$ (b).

References

1. M.De Langlard, H.Al-Saddik, S.Charton, J.Debayle and F. Lamadie. An efficiency improved recognition algorithm for highly overlapping ellipses: Application to dense bubbly flows. *Pattern Recognition Letters*, Elsevier, (101) 88–95, 2018

2. OMS.Ahmad, J.Debayle, N.Gherras, B.Presles, G.Fevotte, and J-C.Pinoli. Quantification of overlapping polygonal-shaped particles based on a new segmentation method of in situ images during crystallization. *Journal of Electronic Imaging,* 21(2), 021115, (2012).

3. S.Rahmani, J-C.Pinoli, and J. Debayle. (2015). Geometrical stochastic modeling and characterization of 2-d crystal population. *Acta Stereologica* (2015)

4. P.Karampelas, J.Kawash, and T.Özyer. *From Security to Community Detection in Social Networking Platforms.* Springer International Publishing, 2019.

5. B.Smith. *Foundations of Gestalt theory,* 1988.

Performance of Digital Image Enhancement Algorithm for Plasmodium Parasite Detection using Thick Blood Smear Digital Microscopic Images

Hanung Adi Nugroho[1], Rizki Nurfauzi[1], Eka Legya Frannita[1]

[1]Department of Electrical and Informatics Engineering, Faculty of Engineering, Universitas Gadjah Mada, 55281 Yogyakarta, Indonesia

Email: adinugroho@ugm.ac.id, rizki.nurfauzi@mail.ugm.ac.id, eka.legya.f@mail.ugm.ac.id

Abstract

Malaria is an infectious disease caused by a bite of a female anopheles mosquito containing the Plasmodium parasite. The spreading of malaria is widely spread in tropical and subtropical countries with a developing economy. A rapid diagnosis is very useful in avoiding the deadly severe symptoms. However, a standard malaria examination is usually conducted manually in which very time-consuming and depends on the medical personnel skills. This condition became a clinical problem for the developing country such as Indonesia. Today, some AI systems for malaria elimination have been successfully developed to overcome the clinical problem of malaria examination. However, they still have some limitations, especially in the data. The quality of input data impacts the trained and the tested model performance. In this study, we developed a Plasmodium detection method by combining GGB (Green-Green-Blue) image enhancement as a feeding step and Faster-RCNN algorithm. We tested the model on a big dataset of thick blood smear digital microscopic images. The dataset contains 2,418 images with 49,900 parasites. We performed the proposed method in several variance of the IoU (intersection over union) thresholds from 0.2 until 0.6. The results show that Faster RCNN combining with GGB image enhancement achieved good performance with sensitivity distinction of (1.34±0.04)% and precision distinction (0.4±0.2) % in all various of IoU thresholds compared with performance of algorithm without image enhancement. Example result can be seen in Fig. 1 and the summary of the proposed method performance in various IoU threshold can be seen in Fig. 2. According to Fig. 2, the highest sensitivity and precision achieved of 83.1% and 88.3% in the testing data, respectively. It indicates that GGB image enhancement is very valuable in increasing the performance of Plasmodium detection and has potential to be implemented in the development of an AI system to support the doctor in making diagnosis decision.

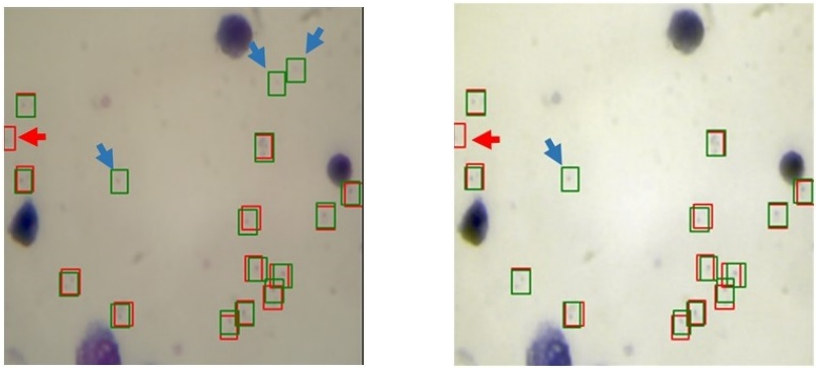

(a) (b)

Figure 1: Comparison results between RGB and GGB image enhancement: (a) example result without any image enhancement technique and (b) example result using GGB image enhancement. Blue point is false positive, red point is false negative, red box is ground truth, and green box is prediction.

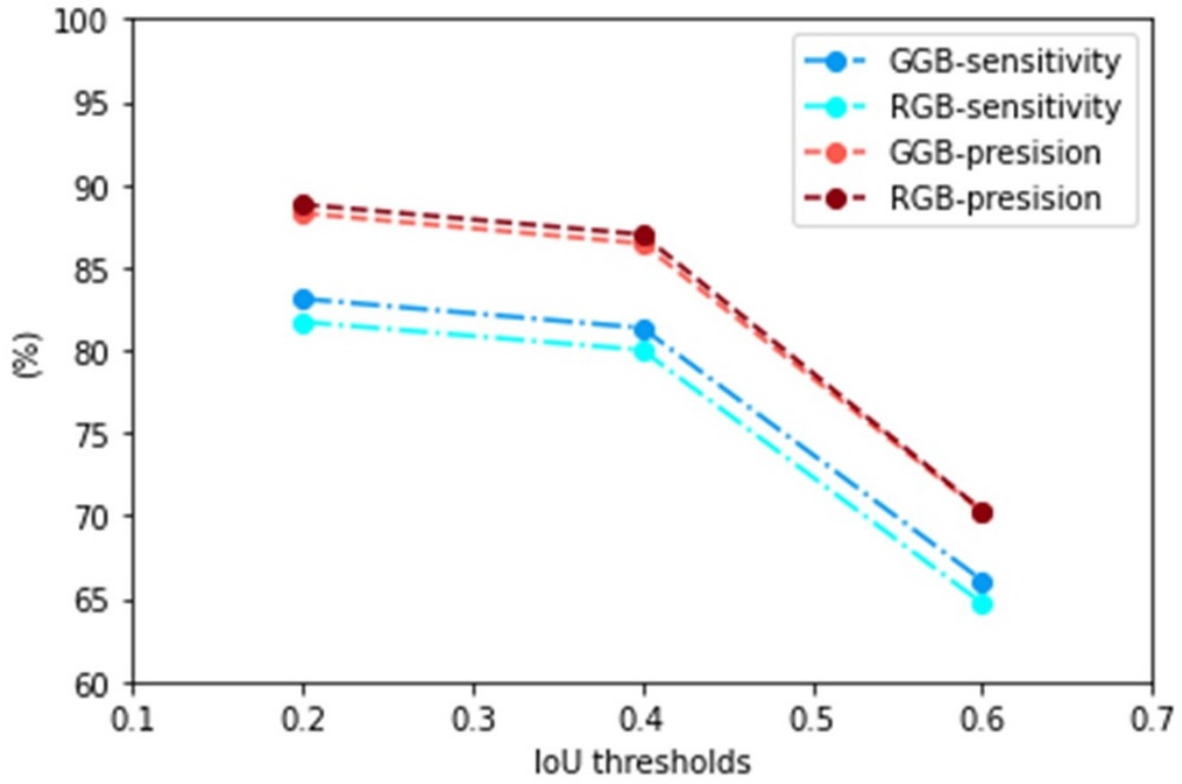

Figure 2: Performance of RGB and GGB in several various of IoU thresholds.

M-tortuosity formalism; from binary to structural and functional characterization

Johan Chaniot[1], Maxime Moreaud[5,7], Loic Sorbier[5], Sébastien A. Lévesque[1], Erik Bélanger[1,3,4], Jean-Marie Becker[6], Thierry Fournel[6], Dominique Jeulin[7], Pierre Marquet[1,2,3]

[1]Centre de recherche CERVO, Université Laval, 2601 Chemin de la Canardière, Québec, QC, G1J 2G3, Canada

[2]Département de psychiatrie et neurosciences, Université Laval, Québec, QC, Canada

[3]Centre d'optique, photonique et laser, Université Laval, 2375 rue de la Terrasse, Québec, QC, G1V 0A6, Canada

[4]Département de physique, de génie physique et d'optique, Université Laval, Québec, QC, Canada

[5]IFP Energies nouvelles, Rond-point de l'échangeur de Solaize, BP 3, 69360 Solaize, France

[6]Université de Lyon, Université Jean Monnet de Saint-Etienne, CNRS UMR 5516, Laboratoire Hubert Curien, F-42000 Saint-Etienne, France

[7]MINES ParisTech, PSL-Research University, CMM, 35 rue Saint Honoré, 77305 Fontainebleau, France

Email: johan.chaniot.1@ulaval.ca, maxime.moreaud@ifpen.fr, loic.sorbier@ifpen.fr, erik.belanger.1@ulaval.ca, jean.marie.becker@univ-st-etienne.fr, fournel@univ-st-etienne.fr, dominique.jeulin@mines-paristech.fr, pierre.marquet@neuro.ulaval.ca

Abstract

Digital image analysis of microstructures has become very important because of the known connections between structural and physicochemical features, in addition to the enhancements of both imaging devices and computational power.
This work deals with a versatile stochastic formalism named the *M-tortuosity* [1]. On the one hand, this formalism is properly defined. On the other hand, a functional version is proposed, named the *F-tortuosity*, aiming to overcome common issues. Segmentation can be a delicate preprocessing step for some applications; characterization of grayscale textures would eliminate the need for accurate segmentation. Real microstructures are usually characterized by a set of descriptors, but separately while local features impact global ones. The *F-tortuosity* provides a solution to mix local features with global topological assessment.
The *F-tortuosity* is based on the functional geodesic distance transform. The functional version τ_f of the morphological tortuosity τ is defined by using a novel notion, the projected functional geodesic distance ($FD^{\perp}_{G}$), as shown in Fig.1(a,b). Except this, the *F-tortuosity* is defined similarly to the *M-tortuosity*, based on a random sampling of N points $\{p_i\}$. The *F-coefficients* associated to each p_i are computed,

$$\hat{C}_n^{-1} = \frac{\sum_{m=0,m\neq n}^{N-1} \frac{1}{FD^{\perp}_{G}(p_m,p_n)^{\alpha_1}}}{\sum_{m=0,m\neq n}^{N-1} \frac{1}{FD^{\perp}_{G}(p_m,p_n)^{\alpha_1}.\tau_{f,n,m}}} \text{ if, } \sum_{m=0,m\neq n}^{N-1} \frac{1}{FD^{\perp}_{G}(p_m,p_n)^{\alpha_1}.\tau_{f,n,m}} \neq 0. \quad (1)$$

The *F-tortuosity* value, i.e., the final *F-scalar*, is then assessed,

$$\hat{\tau}_F = \frac{\sum_{n=0}^{N-1} \epsilon_n \frac{1}{D(p_n,c)^{\alpha_2}}}{\sum_{n=0}^{N-1} \frac{1}{D(p_n,c)^{\alpha_2}.\hat{C}_n^{-1}}} \text{ if, } \sum_{n=0}^{N-1} \frac{1}{D(p_n,c)^{\alpha_2}.\hat{C}_n^{-1}} \neq 0. \quad (2)$$

Additional parameters are present compared to [1,2]: (α_1, α_2) promoting the versatility and ϵ_n increasing the stability against disconnections. The *H_F-tortuosity* is similarly defined but considering the *H-tortuosity* [2].
The main application of this work, considered as a proof of concept, targets the characterization of internal structures of living cells imaged by digital holographic microscopy (DHM), which provides quantitative-phase images, having the great advantage of allowing to visualize, in a non-invasive way, the functional structure of transparent objects such as living cells. Some quantitative-phase images are presented in Fig.1(e), together with synthetic images used for validation purposes (Fig.1(c,d)).

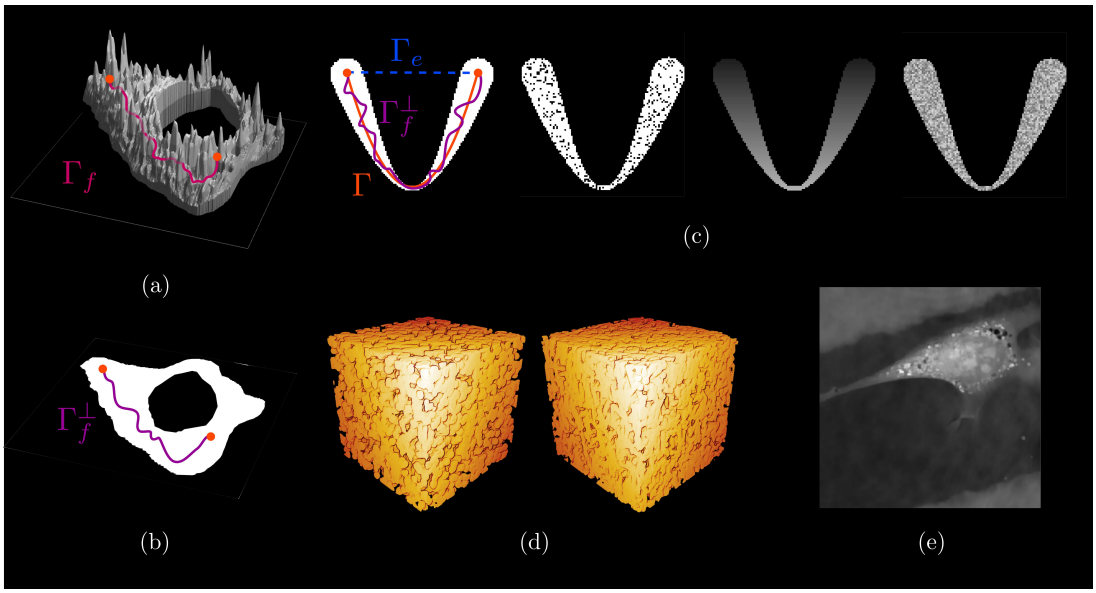

Figure 1: (a-b) Quantitative-phase image of a living cell as in (e), manually segmented (a) with the corresponding mask (b), illustrating the $FD_G^\perp$ represented by the path $\Gamma_f^\perp$ being the orthogonal projection of Γ_f (FD_G). (c) Synthetic image used for validation purposes, two arbitrary points between which are compared different paths: Euclidean Γ_e, geodesic in the binary space Γ and $\Gamma_f^\perp$. (d) Two realizations of Boolean models of spheres (left) and spherocylinders (right). (e) A quantitative-phase image of an immortalized NIH3T3 mouse fibroblast cells ($ATCC\ \#CRL-1658$), obtained by QP-DHM.

References

1. J. Chaniot et al.. Tortuosimetric operator for complex porous media characterization. *Image Analysis & Stereology* **38** (1), 25–41, 2019.

2. J. Chaniot et al.. Heterogeneity assessment based on average local variations of geometric tortuosity for complex porous structures characterization. *Image Analysis & Stereology* **39** (1), 111–128, 2020.

Birth and death simulation of human corneal endothelium cells

Gilles Thuret[1], Z. He[1], H. Vaitinadapoule[1], O. Ben Moussa[1], A. Amri[1], J. Thomas[1], F. Mascarelli[1], P. Gain[1], Yann Gavet[2]

[1]Laboratoire Biologie, ingénierie et imagerie de la Greffe de Cornée (BiiGC), Faculté de Médecine, Campus Santé Innovation, Université Jean Monnet, Saint-Etienne, France.
[2]Mines Saint-Etienne, Univ. Lyon, CNRS, UMR 5307 LGF, Centre SPIN, F - 42023 Saint-Etienne, France.

Email: gavet@emse.fr

Abstract

The human corneal endothelium, the most posterior layer of the cornea, is a monolayer of flat cells that are perfectly joined and are essential for maintaining its transparency over time. Long considered to be non-regenerative in adults, several recent studies have nevertheless shown that some cells can proliferate in the periphery of the endothelium. At birth, the endothelial cell density (ECD, number of cells per unit area) is very high and the endothelial mosaic consists of perfect hexagons. During life, some cells disappear, others divide and the mosaic reorganizes itself: its polymorphism and polymegethism increase. Thus, after 20 years, the central WFD decreases by 0.6% per year, remaining higher in the periphery. However, endothelial homeostasis remains poorly understood, in particular how new peripheral cells partially compensate for the disappearance of other more central cells. The cells form a regular pavement, which can be considered mathematically as a Voronoi pavement without holes. We simulated the organization and reorganization of the cells by means of a centered Voronoi diagram, which was created iteratively by moving the seeds of the diagram to the geometric center of the cells. The initialization of the seeds was done with a uniform distribution, and a few centering iterations were sufficient to have cells close to hexagons. Subsequently, we simulated the evolution through cycles of cell death/birth, followed by cell centering. This new simulation tool will allow us to test many hypotheses on the number and frequency of cellular events (mitosis and death) in order to elucidate endothelial pathophysiology.

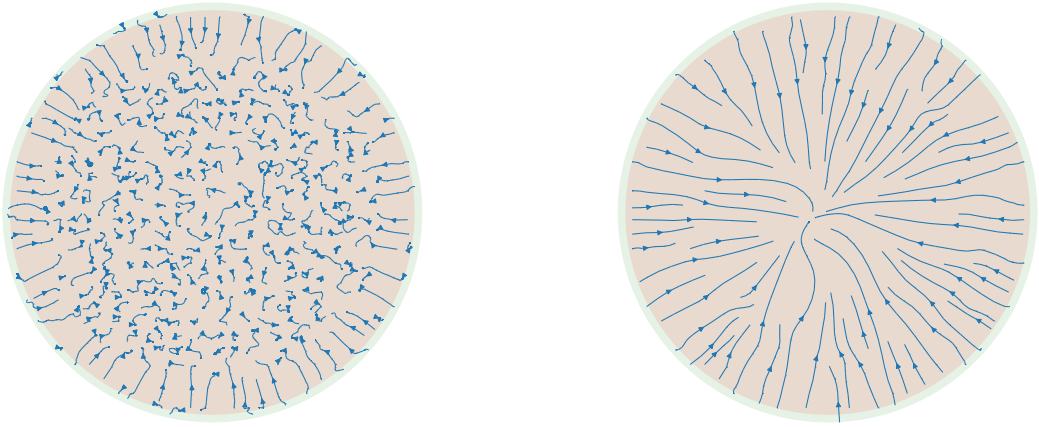

Figure 1: Stream lines showing the centripetal migration of the cells from early (left) to late stage (right).

Estimation of summary characteristics for random closed sets

Zbyněk Pawlas

Department of Probability and Mathematical Statistics, Faculty of Mathematics and Physics, Charles University, Sokolovská 83, 186 75 Prague, Czech Republic

Email: pawlas@karlin.mff.cuni.cz

Abstract

Random closed sets serve as useful mathematical models to describe complex geometrical structures in the d-dimensional Euclidean space. The distribution of a random closed set Ξ is uniquely determined by its capacity functional $T_\Xi(K) = \mathbb{P}(\Xi \cap K \neq \emptyset)$, defined for compact $K \subseteq \mathbb{R}^d$. Simpler summary characteristics can be derived from the capacity functional. For example, for a stationary random closed set Ξ, the volume fraction $p = T_\Xi(\{x\})$ is independent of $x \in \mathbb{R}^d$, the two-point probability function $C(x-y) = 2p - T_\Xi(\{x,y\})$ depends only on $x-y$, and the spherical contact distribution function $H(r) = 1 - \frac{1-T_\Xi(b(x,r))}{1-p}$ is independent of $x \in \mathbb{R}^d$. We study statistical properties of non-parametric estimators of these characteristics. A particular interest is in asymptotic behaviour. We also consider extensions for bivariate and marked random closed sets. The estimators could be used for testing the hypothesis that the components of a bivariate random closed set are independent or the hypothesis that the marks are independent of the underlying set in a random marked closed set.

Morphological models characterization: a Bayesian approach

Bruno Figliuzzi
Center for Mathematical Morphology
Mines Paris - PSL Research University

Materials often present a complex internal microstructure, which largely determines their physical properties at the macroscopic level [3]. A common way to study the microstructure influence on the macroscopic properties of materials is to generate random structures that accurately reproduce the geometrical characteristics of the microstructure. These simulated microstructures can subsequently be used to analyze the physical or mechanical properties of heterogeneous materials through extensive numerical simulations [2]. This approach is particularly efficient to identify microstructures yielding optimized functional properties for specific applications.

Stochastic geometry models [1] are classically used to describe microstructures observed in heterogeneous materials. Usually, these models depend upon a set of parameters Θ, that must be chosen carefully to match the experimental observations conducted on the microstructure of the material. A common approach to perform the parameters determination is to try to minimize an objective function, usually taken to be the discrepancy between measurements computed on the simulations and on the experimental observations, respectively.

Several methods are considered in the literature to perform the minimization task. A classical solution is to use a gradient descent algorithm. Gradient descent algorithms are very efficient to perform the minimization of strongly convex functionals and are extensively used in a number of fields. Nevertheless, several difficulties are associated with these methods when applied to the problem considered here. Firstly, for morphological models, the computation of the objective function gradient is often untrackable analytically, and one has therefore to rely on a finite difference scheme to evaluate the gradient at each iteration of the descent algorithm. At each step, this requires to compute at least $D + 1$ evaluations of the objective function, D being the dimension of the parameters space. In addition, the intrinsic sta-

tistical variability of the morphological models often leads to noisy estimates of the gradient. Secondly, the objective function that one seeks to minimize is often non-convex, which means that a gradient descent algorithm will only converge toward a local minimum of the objective function.

Several alternatives to the gradient descent algorithm have been proposed in the literature. In [2], the authors notably propose to conduct the optimization procedure by employing the Nelder-Mead algorithm. The Nelder–Mead algorithm is an heuristic that can be used to determine the minimum or maximum of an objective function in a multidimensional space. It is a direct search method that only relies upon iterative evaluations of the objective function, and which can therefore be applied to problems for which the computation of the gradient is not trackable analytically.

In this communication, we present a Bayesian approach for determining the parameters of the morphological model according to a posterior distribution model. A Monte Carlo Markov Chains (MCMC) algorithm allows us to generate samples from the posterior distribution. This approach presents several advantages when compared to other methods. In particular, the MCMC approach allows to obtain samples that reproduce the actual posterior distribution. We show on several examples that the Bayesian approach allows to properly identify the optimal parameters of a morphological model and to identify potential correlations between model parameters.

References

[1] Sung Nok Chiu, Dietrich Stoyan, Wilfrid S Kendall, and Joseph Mecke. *Stochastic geometry and its applications*. John Wiley & Sons, 2013.

[2] Bruno Figliuzzi, Dominique Jeulin, Matthieu Faessel, François Willot, Masataka Koishi, and Naoya Kowatari. Modelling the microstructure and the viscoelastic behaviour of carbon black filled rubber materials from 3d simulations. *Technische Mechanik*, 32(1-2):22–46, 2016.

[3] Joachim Ohser and Katja Schladitz. *3D images of materials structures: processing and analysis*. John Wiley & Sons, 2009.

Random tessellations marked with crystallographic orientations

Iva Karafiátová[1], Zbyněk Pawlas[1], Luděk Heller[2]

[1]Department of Probability and Mathematical Statistics, Faculty of Mathematics and Physics, Charles University, Sokolovská 83, 186 75 Prague, Czech Republic

[2]Institute of Physics of the Czech Academy of Sciences, Na Slovance 2, 182 21 Prague, Czech Republic

Email: karafiatova@karlin.mff.cuni.cz

Abstract

In paper [2] we consider a random marked tessellation in which the marks are crystal lattice orientations. The task is to construct a statistical test to decide whether the orientations are independently assigned to the cells of the underlying tessellation. The distribution of a given orientation is either identical for all cells or may depend on the corresponding cell. For both cases, non-parametric tests are developed. Using simulations, power computations are conducted for alternative models with different forms of mark correlation. The alternative models of orientations are generated from more sophisticated probability distributions than we presented at the paper. Also, we demonstrate the application in the analysis of 3D polycrystalline materials with cubic crystal symmetry.
In addition we consider other sets of marks, grain-wise averaged stress and standard deviations of stress within a single grain, which can be for cubic crystal symmetry represented as three by three real matrices. The task is to study the dependence between these marks. Additionally we can consider grain volumes or the information about the grain boundaries. To do so, we perform independence tests presented in [1,3]. In case of rejecting the null hypothesis about the independence, further analysis follows. The next step is to model the expected values of standard deviations within single grains by knowledge of the dependencies between the stress values and the microstructure.

References

1. R. Lyons. Distance covariance in metric spaces. *The Annals of Probability*, **41**(5):3284–3305, 2013.

2. Z. Pawlas, I. Karafiátová and L. Heller. Random tessellations marked with crystallographic orientations *Spatial Statistics*, **39**, 100469, 2020.

3. G.J. Székely, M. L. Rizzo, and N. K. Bakirov. Measuring and testing dependence by correlation of distances. *The Annals of Statistics*, **35**(6):2769–2794, 2007.

Sensitivity of the local measures to deviations of the typical grain shape in Boolean models.

Tatyana Eremina[1], Johan Debayle[1], Frédéric Gruy[1], Jean-Charles Pinoli[1]

[1]MINES Saint-Etienne, CNRS, UMR 5307 LGF, Centre SPIN, 158 cours Fauriel, SAINT-ETIENNE Cedex 2 42023, France

Email: tatyana.eremina@emse.fr, debayle@emse.fr, fgruy@emse.fr, pinoli@emse.fr

Abstract

The method of the typical grain elongation ratio estimation based on the local measures distributions is proposed. The local measures are straightforward generalizations of the Minkowski functionals (MFs) (in $\mathbb{R}^2$ coincide up to normalization with classical geometric measurements: Euler-Poincaré characteristic, perimeter and area). Consider a random structure $\tilde{\Xi}$ in $\mathbb{R}^d$, and take values of the Minkowski functionals for $\tilde{\Xi} \cap B_r(\tilde{x})$, where $B_r(\tilde{x})$ is a ball of radius r positioned in a uniformly randomly distributed point $\tilde{x}$. For the different realizations of $\tilde{x}$ the different values are obtained, which provide $d+1$ measures in the sense of the measure theory: mappings which assign real numbers to sets and which become "random measures" [1, ch. 7]. These localizations of MFs previously were used to characterize the porous structure of a Fontainebleau sandstone [2].
The local measures distribution estimation is applied to the particular random spatial structures - homogeneous Boolean models (BM) of rectangles uniformly randomly oriented and with a fixed and random elongation ratio. The sensitivity of the local measures (see Fig.1) to deviations of the elongation ratio of the typical grain allows it to be estimated. For simulated random spatial structures with the area density from 0.2 to 0.9, the error in the estimation of the elongation ratio is $< 10\%$ at 100 realizations of a random structure and $< 5\%$ at 500. Same was true even at the high area density, when most particles overlap and the local analysis of the spatial structure is complicated. It has been shown that the nature of the elongation ratio (fixed or random) has a little influence on the accuracy of the estimation as long as the number of the random spatial structure realizations is big enough.

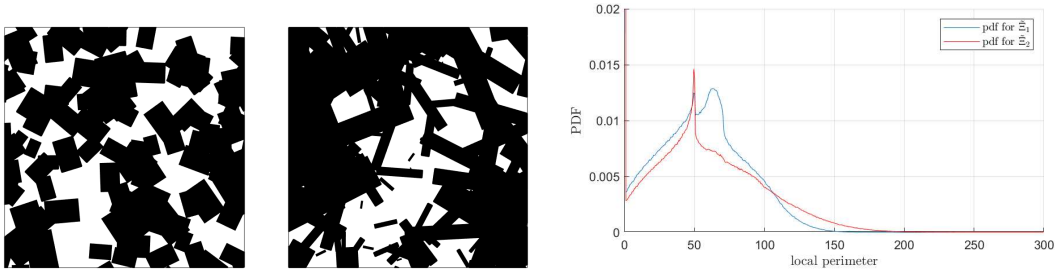

(a) BM $\tilde{\Xi}_1$ (b) BM $\tilde{\Xi}_2$ (c) local perimeter measure

Figure 1: (a),(b) Realizations of two homogeneous Boolean models of rectangles with different elongation ratio. The global measures remain equal (equal MF densities – area density, perimeter density and specific Euler-Poincaré characteristic), and equal intensity of the underlying point process. Only the typical grain parameters change. (c) Probability density functions of the local perimeter measure compared for BMs of rectangles $\tilde{\Xi}_1$ and $\tilde{\Xi}_2$.

References

1. Arns CH, Mecke J, Mecke K, Stoyan D (2005). Second-order analysis by variograms for curvature measures of two-phase structures. Eur Phys J B 47:397-409.

2. Chiu SN, Stoyan D, Kendall WS, Mecke J (2013). Stochastic geometry and its applications: John Wiley & Sons.

Comparison of segmentation of 2D and 3D EBSD measurements in polycrystalline materials

J. Stanek[1], J. Kopecek[2], P. Kral[3], I. Karafiatova[4], F. Seitl[4], V. Benes[4]

[1]Department of Mathematics Education, Faculty of Mathematics and Physics, Charles University, Sokolovská 83, 186 75 Prague, Czech Republic,
[2]Institute of Physics of the CAS, Department of Functional Materials, Na Slovance 2, 18200 Prague, Czech Republic,
[3] Institute of Physics of Materials of the CAS, Zizkova 22, 61662 Brno, Czech Republic,
[4]Department of Probability and Mathematical Statistics, Faculty of Mathematics and Physics, Charles University, Sokolovská 83, 186 75 Prague, Czech Republic

Email: stanekj@karlin.mff.cuni.cz, kopecek@fzu.cz, pkral@ipm.cz, karafiatova.iva@gmail.com, seitl@karlin.mff.cuni.cz, benesv@karlin.mff.cuni.cz

Abstract

While classical stereology of polycrystalline materials dealt with 2D metallographic sections of the specimen, nowadays thanks to modern microscopy, e.g. electron backscatter diffraction (EBSD) we may have access to voxelized 3D stack of data. Nevertheless in some laboratories still 2D EBSD is used. A comparison study of grain segmentation in 2D and 3D EBSD, based on a misorientation threshold, is presented [1]. Using Laguerre tessellations with orientation marks, a simulation study that demonstrates a different sensitivity of segmentation in the case of low angle and high angle grain boundaries is involved. Then two metallic materials measured by 3D EBSD are investigated concerning segmentation, and there are given some recommendations for the misorientation thresholds. Computational tools such as DREAM 3D software enable efficient data evaluation that is completed by a five-parameter analysis of grain boundaries.

References

1. J. Stanek, J. Kopecek, P. Kral, I. Karafiatova, F. Seitl, V. Benes. Comparison of segmentation of 2D and 3D EBSD measurements in polycrystalline materials. *Kovove Materialy* **58**, 301–319, 2020.

Lycopene increases the number of osteocytes in the femur of female rats with osteoporosis.

[1]Mayara Sgarbi Semeghini, [2]A. Augusto Coppi, [1]Selma Siessere, [1]Karina Fittipaldi Bombonato-Prado

[1]Bone Research Lab, Department of Basic and Oral Biology, School of Dentistry of Ribeirão Preto, University of São Paulo, Ribeirão Preto, SP, Brazil

[2]School of Animal, Rural and Environmental Sciences, Nottingham Trent University, Brackenhurst Campus, Nottingham, NG25 0QF, United Kingdom

Email: augusto.coppi@ntu.ac.uk

Abstract

Osteoporosis is a prevalent disease with high incidence in women at the onset of menopause mainly because of hormonal changes, genetics and lifestyle, leading to decreased bone mass and risk of fractures. Maintaining bone mass is a challenge for women in this period of life and nutrition counts for calcium rich food intake. Nevertheless, other nutrients such as carotenoids may influence bone metabolism because of its high antioxidant properties. The aim of this study was to evaluate the effect of carotenoid lycopene on bone cells and in the microarchitecture of ovariectomized rats by means of in vitro assays. Daily ingestion of 10 mg/kg of lycopene by gavage for 8 weeks after ovariectomy was conducted for stereological evaluation of number and volume of osteocytes of femur distal epiphysis. After 8 weeks of ovariectomy, femurs were removed. Oral administration of lycopene did not influence microarchitecture of femoral epiphysis, but increased the total number of osteocytes in the ovariectomized rats. Results suggest that lycopene promotes positive changes in bone metabolism with the onset of osteoporosis.

Key words: Lycopene, Osteoporosis, Design-based Stereology

Stochastic models for polycrystalline materials

Filip Seitl[1]

[1]Department of Probability and Mathematical Statistics, Faculty of Mathematics and Physics, Charles University, Sokolovská 83, 186 75 Prague, Czech Republic

Email: seitl@karlin.mff.cuni.cz

Abstract

In materials research the microstructure of polycrystalline alloys plays a crucial role in behaviour of the material. Modern microscopy enables to obtain three-dimensional data from a material specimen in a voxelized form, i.e., as a digitalized 3D image. The basic units of the material, grains, are described by a mathematical model of 3D tessellation. In the talk the focus will be devoted to the tessellations allowing a representation by a set of seeds called generators. The basic concept of a Voronoi tessellation [1], where the generators are just spatial locations, is not enough flexible to model real polycrystals. A wider class of Laguerre tessellations [2], adding a positive weight to each spatial location, is frequently used in this field.

The voxelized data are fitted by a tessellation using optimization techniques such as linear programming, cross entropy, [3], or simulated annealing, [4]. A desirable task is to find a stochastic model suitable to represent data of a given polycrystalline material. This is certainly useful when producing the material repeatedly by means of a given technological process. As the tessellation is determined by the sets of generators, the task reduces to searching for a suitable model for a (marked) point process of generators. The marked point process of generators of the Laguerre tessellation has typically dependent marks [5]. This exludes the possibility of independent or geostatistical marking. Both spatial locations and weights (=marks) have to be modelled simultaneously. Different approaches will be discussed, among them especially Gibbs point process model, [6], and statistical reconstruction of point processes, Section 6.7. in [7] .

References

1. A. Okabe, B. Boots, K. Sugihara, S. N. Chiu and D. G. Kendall. *Spatial Tessellations: Concepts and Applications of Voronoi Diagrams.* John Wiley & Sons 2000.

2. C. Lautensack and S. Zuyev. Random Laguerre tessellations. *Advances in Applied Probability* **40** (3), 630–650, 2009.

3. A. Spettl, T. Brereton, Q. Duan, T. Werz, C. E. Krill III, D. P. Kroese and V. Schmidt. Fitting Laguerre tessellation approximations to tomographic image data. *Philosophical Magazine* **96** (2), 166–189, 2016.

4. O. Šedivý, T. Brereton, D. Westhoff, L. Polívka, V. Beneš, V. Schmidt and A. Jäger. 3D reconstruction of grains in polycrystalline materials using a tessellation model with curved grain boundaries. *Philosophical Magazine* **96** (18), 1926–1949, 2016.

5. D. Stoyan, F. Seitl and V. Beneš. Dependent radius marks of Laguerre tessellations: a case study. To appear in *Australian & New Zealand Journal of Statistics* 2021. DOI: 10.1111/anzs.12314.

6. F. Seitl, L. Petrich, J. Staněk, C. E. Krill III, V. Schmidt and V. Beneš. Exploration of Gibbs-Laguerre tessellations for three-dimensional stochastic modeling. *Methodology and Computing in Applied Probability*, Online First, 2020. DOI: 10.1007/s11009-019-09757-x.

7. J. Illian, A. Penttinen, H. Stoyan and D. Stoyan. *Statistical Analysis and Modelling of Spatial Point Patterns.* John Wiley & Sons 2008.

Oxide characterization using sparse unmixing

Tarek Zenati[1,2], Bruno Figliuzzi[1], Grace Shu-Hui Ham[2]

[1] Center for Mathematical Morphology, Mines Paris, PSL Research University

[2] ArcelorMittal Research, Maizières-lès-Metz, France

Email: tarek.zenati@mines-paristech.fr, bruno.figliuzzi@mines-paristech.fr, grace.ham@arcelormittal.com

Abstract

Hyperspectral sensors are increasingly being used for quality control in the industry. In particular, they provide a potential way to detect the formation of oxide defects on steel surfaces and to characterize the chemical composition of these defects [1]. Hyperspectral sensors collect information in the form of a set of L spatial images, where each individual image corresponds to a spectral band of the electromagnetic spectrum. The spatial resolution is an essential feature of the sensors: when the spatial extent of a pixel is wide, the observed spectrum is usually a combination of the spectra of the different chemical species present in the observed region. To discern defects that occur at a scale smaller than the pixel size, a key issue is the unmixing of the elementary spectra present in the observations [2]. Indeed, a good unmixing algorithm provides reliable information on the acquired data, and therefore allows to detect defects with great precision. Oxide concentrations and quantitative information such as their thickness can be deduced accurately if unmixing is appropriately applied.

In this presentation, we present a semi-supervised unmixing algorithm based upon an optical model describing the spectra formation [3]. In particular, we describe how we use the optical model to understand the interactions that are occuring between the light and the chemical species. In the optical model, we make the explicit assumption that several oxide layers are stacked together on a steel substat. We rely on the Drude-Lorentz model to compute the complex permittivity of each layer of oxide. Next, we describe the light propagation through the stacked layers by computing a characteristic matrix, which depends on the incidence angle of the incoming light, on the oxide present in the stacked layers and on the respective thicknesses of the layers. Knowing the chemical composition and the thickness of each oxide layer, it becomes straightforward with the optical model to compute the reflected spectra.

In this study, our aim is to study the inverse problem, which corresponds to the determination of the chemical composition and of the thickness of the oxide layers from the observation of a reflected spectrum s. To that end, we rely on a semi-supervised approach where we precompute K optical responses of multi-layers with distinct thicknesses and chemical compositions. These optical responses are then stored in a K by L dictionary matrix D. Then, we try to determine the linear combination of spectra from the dictionary that reproduces s with a minimal specified accuracy ϵ while using the least possible number of spectra in D. This boils down to solve the convex optimization problem [4]:

$$\hat{\alpha} = \arg\min_{\alpha \in R^K} \|a\|_{L^1} \quad s.t. \quad \|s - Da\|_{L^2} \leq \epsilon. \tag{1}$$

By solving (1), we demonstrate on numerical examples that it is possible to recover the thicknesses and the composition of the oxide layers.

The effects of diabetes type 2 on capillary network of inspiratory muscles analysed by a 3D method

Rok Tit Tomazin[1], Erika Cvetko[1], Armin Alibegović[2], Janáček Jiří[3], Nejc Umek[1]

[1] Institute of Anatomy, Faculty of Medicine, University of Ljubljana, Korytkova ulica 2, 1000 Ljubljana, Slovenia
[2] Institute of Forensic Medicine, Faculty of Medicine, University of Ljubljana, Korytkova ulica 2, 1000 Ljubljana, Slovenia
[3] Department of Biomathematics, Institute of Physiology, Czech Academy of Science, Vídeňská 1083, 14220 Prague 4, Czech Republic
Email: nejc.umek@mf.uni-lj.si

With an estimated global prevalence of 463 million people in 2019, diabetes mellitus is one of the leading causes of morbidity and mortality worldwide, and especially in the developed world. Skeletal muscles and the microvasculature have been shown to play critical roles in the pathophysiology of type 2 diabetes and other insulin-resistant states. In advanced obesity with insulin resistance, a decrease in the density of skeletal muscle capillary network and impaired capillary recruitment have been demonstrated in weight bearing limb muscles [1]. Conversely, more recent studies of obesity and insulin resistance in animal models described an increase in the skeletal muscle capillary network [2]. It is likely that insulin resistance may have differential effect on different skeletal muscle functional types. While the functional effect of obesity and diabetes on respiratory muscles has been described [3], the effect on the morphology of their capillary network is less known. Capillarization of skeletal muscles is usually assessed with two-dimensional (2D) analyses of tissue cross-sections. However, because this conventional method can have a systematic error of up to 75%, Eržen et al. have developed a more accurate but very demanding three-dimensional (3D) method of capillary network analysis [4,5]. Accordingly, the aim of our study was to investigate the changes of capillary network around individual muscle fibres of human inspiratory muscles diaphragm and external intercostal muscles.

This 3D method for studying capillaries involves marking of 100 µm thick tissue sections of skeletal muscle with fluorescent antibodies. Muscle fibres are marked with antibodies against collagen IV, while capillaries are marked with antibodies against Von Willenbrand factor and with fluorescently marked lectin. Stacks of images are captured using a confocal microscope with 1 µm distance between the images. The axial calibration of individual image stacks is corrected for shrinkage and images are segmented by thresholding. Following skeletonization of the binary image with a six-pass Palagyi algorithm, the result is vectorized to a 5 µm line segment geometric graph and manually corrected in virtual reality using a haptic device. The muscle fibre diameter, surface area, and volume are calculated from the muscle fibre outlines, which are delineated manually on optical sections at four levels within the stack. The capillary network around a single muscle fibre is evaluated using different indices. The estimated capillary length is expressed as the sum of the line segment lengths around an individual fibre, and defined per muscle fibre length, surface area, and volume. Tortuosity is expressed as the sum of exterior angles (in radians) between successive line segments per total capillary length.

Using the described method, we studied the capillarisation of the diaphragm and the external intercostal muscles in autopsy samples of 16 adult males, 8 of which were obese (BMI > 30 kg/m2) and had a 10-year history of type 2 diabetes without complications and 8 age-matched non-diabetic lean controls (BMI < 25 kg/m2). Muscle samples were taken during routine autopsies and medical

records were checked to exclude all individuals with neuromuscular disorders, pharmaceutical therapy, prolonged immobilisation, and other factors that could possibly affect muscle capillarisation.

In diabetic individuals, the external intercostal muscles were significantly better capillarised than in non-diabetic controls, while there were no significant differences in capillarisation of the diaphragm between the study groups. Furthermore, the capillaries in the external intercostal muscles of diabetic individuals were significantly less tortuous and more anisotropic compared to non-diabetic controls. The differences in capillarisation were greater around large muscle fibres with diameter larger than 45 µm than around small muscle fibres. Similarly, the capillary supply of the diaphragm around small and large muscle fibres showed the same trends in all parameters, although the results were not statistically significant. There were no differences in muscle fibre diameters between the two studied groups or between the two studied muscles.

Our results show that in type 2 diabetes without complications, the capillary supply of respiratory muscles is increased, which could be a compensatory mechanism of the organism to ameliorate the effects of insulin resistance. Furthermore, we have observed greater changes in the capillary network of the external intercostal muscles compared to the diaphragm. A possible explanation is that the diaphragm is a continuously active, slow-twitch muscle that is more resilient to the effects of diabetes compared to external intercostal muscles which generally activate only during strenuous breathing, the Valsalva manoeuvre etc. Nonetheless, while not statistically significant, the changes observed in the diaphragm follow the same pattern as in the external intercostal muscle leaving open the possibility that no significant changes were observed due to the small number of studied individuals in this preliminary study.

Funding
This study was supported by Slovenian research agency (Grant No. P3-0043) and the Czech-BioImaging large RI project (LM2015062 funded by MEYS CR) and European Regional Development Fund Project- (No. CZ.02.1.01/0.0/0.0/16_013/0001775).

References

1. T. P. J. Solomon, J. M. Haus, Y. Li and J. P. Kirwan. Progressive hyperglycemia across the glucose tolerance continuum in older obese adults is related to skeletal muscle capillarization and nitric oxide bioavailability. *J. Clin. Endocrinol. Metab.* **96** (5), 1377–1384, 2011.
2. N. Umek *et al.* 3D analysis of capillary network in skeletal muscle of obese insulin-resistant mice. *Histochem. Cell Biol.* **152** (5), 323–331, 2019.
3. C. C. W. Hsia and P. Raskin. Lung function changes related to diabetes mellitus. *Diabetes Technol. Ther.* **9** (1), 2007.
4. I. Erzen. A novel staining method. *Eur. J. Histochem.* **48** (2), 151–158, 2004.
5. J. Janáček, E. Cvetko, L. Kubínová, L. Travnik and I. Eržen. A novel method for evaluation of capillarity in human skeletal muscles from confocal 3D images. *Microvasc. Res.* **81** (2), 231–238, 2011.

Stereology of Liver after Sucralose ingestion: Effect and possible hypothesis

Diwakar Dhurandhar
Associate Professor, Department of Anatomy, Pt. J.N.M Medical College, Raipur, Chhattisgarh, India
Email: diws.dhurandhar@gmail.com

Abstract

Introduction: Sucralose is a non-caloric artificial sweetener which is very commonly available in the nearest provision store in the name of Splenda or Sugar free Natura. It was approved by FDA in 1999 as general purpose sweetener. It is liked for its ideal Metabolic and Chemical properties. Thus, loved by diabetics and fitness conscious groups alike. Reduction in the amount of good bacteria in intestines of rats by 50% along with increase in pH level, Body weights and Levels of p-glycoprotein have been reported in rats when consumption ranged between 1.1-11mg/kg/day. Liver is detoxification organ of the body and most of sucralose gets concentrated in the liver. Any chlorocarbon ingested can cause interference in the metabolism and damage to organs of the body. Though Histopathology and Histomorphometry after ingestion of sucralose was done by the present author, Stereology has not been reported to the best of our knowledge.

Aim and Objectives:

To evaluate the stereological parameters of livers of albino rats in Sucralose treated rats and compare with distilled water treated rats with special reference to:

1. Volume of total liver, sinusoids and Parenchyma.
2. Mean Numerical Density and Number of hepatocytes.
3. Mean Numerical Density and Number of binucleated hepatocytes.
4. Mean Diameter of nuclei of Hepatocytes.

Material and Methods:

Twelve rats were divided into Experiment group having six rats treated with 3 g/kg/day dissolved in distilled water via oral gavage for 30 days and Control Group given equal volume of Distilled water.

Systematic Uniform random sampling: Four pieces each having thickness of 5mm were taken for paraffin sectioning from four lobes of rat liver. 5µ thick sections were cut using rotary microtome. Observations of H & E slides of 6 control rats were statistically compared with those of Experimental rat slides using independent T test or Non parametric Mann Whitney U test using SPSS version 21.0

Estimation of Volume of Liver, Sinusoids and Parenchyma was done using Cavalieri Point counting technique whereas estimation of Mean Numerical Density was done using Physical Dissector Method. Total number of hepatocytes is obtained by Multiplying Mean Numerical density with Volume. All the Stereological parameters were estimated using Stepanizer version β 2.28.

Conclusions and Discussion: Total volume of the liver in the Sucralose treated group was increased significantly compared to controls. Sinusoidal dilatation and connective tissue fibrosis has already been reported by present authors after exposure with sucralose. The reduced number of hepatocytes was caused by degeneration and death of these cells. These finding has already been reported by present author. The mean numerical density and total number of binucleated hepatocytes were increased significantly in the sucralose treated group compared to untreated controls. The nuclear nuclear diameter of hepatocytes was significantly decreased. This might be due to alteration of the genetic material including pyknotic or heterochromatic changes.

Table 1 STEREOLOGICAL PARAMETERS

ESTIMATION	CONTROL	CE	SUCRALOSE	CE	P value
Liver volume (cm^3)	9.61 ± 1.32	0.003	12.009 ± 2.21	0.002	**<0.01**
Volume of parenchyma	6.54 ± 2.39	0.013	5.46 ± 1.21	0.034	**<0.01**
Volume of sinusoids	3.43 ± 0.98	0.02	5.65 ± 1.9	0.027	**<0.01**
Nuclear Density of Hepatocytes per mm^3	$234.26 \times 10^3 \pm 1367$	0.02	$172.67 \times 10^3 \pm 1354$	0.012	**<0.01**
Nuclear Density of BN Hepatocytes per mm^3	$30.23 \times 10^3 \pm 763$	0.04	$39.61 \times 10^3 \pm 729$	0.001	**<0.05**
Total no of hepatocytes	$2.65 \times 10^6 \pm 102354$	0.02	$1.54 \times 10^6 \pm 127854$	0.001	**<0.05**
Total no of BN hepatocytes	$278.32 \times 10^3 \pm 16734$	0.01	$439 \times 10^3 \pm 26734$	0.02	**<0.01**
Diameter of Hepatocytes	7.9 ± 0.87	0.01	5.11 ± 0.43	0.03	**<0.01**

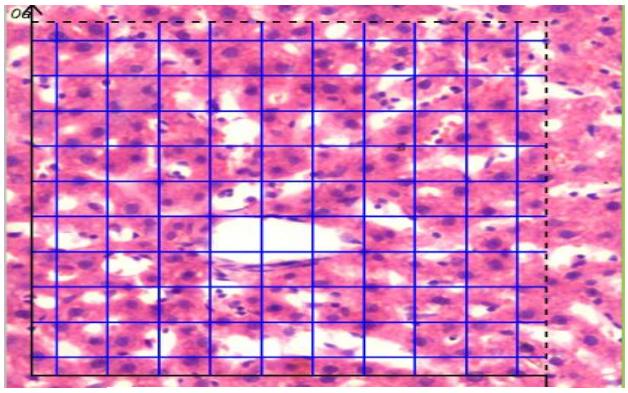

Figure 1 POINT COUNTING GRID FOR CAVALIERI PRINCIPLE

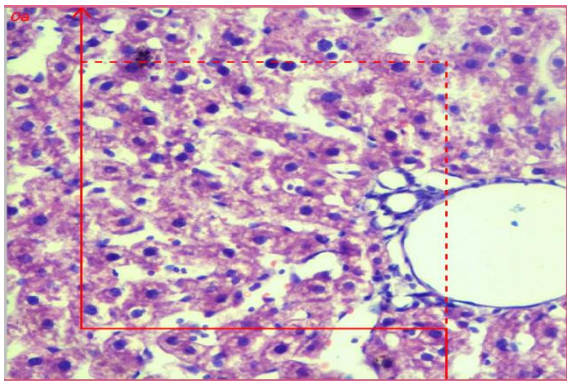

Figure 2 PHYSICAL DISSECTOR PRINCIPLE TO ESTIMATE THE NUMERICAL DENSITY OF THE HEPATOCYTES

References:

1. Knight I. The development and applications of sucralose, a new high intensity sweetener. Can J Physiol Pharmacol 1994;72:435—9.
2. Abou-Donia MB, El-Masry EM, Abdel-Rahman AA, McLendon RE, Schiffman SS. Splenda alters gut microflora and increases intestinal p-glycoprotein and cytochrome p-450 in male rats. J Toxicol Environ Health A 2008;71:1415—29.
3. Dhurandhar D, Bharihoke V, Kalra S. A histological assessment of effects of sucralose on liver of albino rats. Morphologie. 2018 Sep;102(338):197-204. doi: 10.1016/j.morpho.2018.07.003. Epub 2018 Aug 2. PMID: 30078469.
4. A Yahyazedeh, BZ Altunkaynak, N Akgül & HM Akgül (2017): A histopathological and stereological study of liver damage in female rats caused by mercury vapor,Biotechnic & Histochemistry, DOI: 10.1080/10520295.2017.1312527
5. Sterio DC. (1984) The unbiased estimation of number and sizes of arbitrary particles using the disector. J.Microsc. 134, 127–136

Characterization of Pyramidal Cells in Layer III of Brodmann Area 46 in Schizophrenia and Depression

Larsen Nick Y.[1], Nyengaard Jens Randel[1]

[1]Aarhus University, (Aarhus, Denmark)

Email:

Abstract

In recent years, techniques involving three-dimensional (3D) reconstruction of cells and tissue structure have been the subject of increased interest for a better understanding of the relationship between structure and function. However, our understanding of the association between the brain's structure and function remains limited, particularly when compared with other organ systems. Imaging techniques have shown that patients with schizophrenia and depression have brain abnormalities in Brodmann Area 46 (BA46).
We designed an automated approach that allows us to assess pyramidal cells and their spatial organization in layer III of BA46 in archived human brain tissue using the most recent 3D tissue reconstruction and cellular analysis.
In 3D, the morphological data revealed information on the number density, volume, sphericity, orientation and diameter. For spatial point pattern analysis of 3D datasets, an empirical approach known as the cylindrical K-function was used to analyze the neural organization. In addition to obtaining the 3D structural changes and organization, we employed stereology to estimate total volume of layer III in BA46, total pyramidal cell number and density. Volume tensors obtained via the planar rotator quantified volume, shape and orientation of pyramidal cells.
The findings revealed variations in pyramidal cell quantities of layer III in BA46, where it was mainly decreased for schizophrenic patients. We also discovered that the positions of neurons are either arranged into columnar structures or have some repulsive behavior against each other. Our pipeline may be used to solve challenges in developmental biology and disease that require sufficient identification of cells or other structures.

MINES Saint-Étienne

Une école de l'IMT

issia

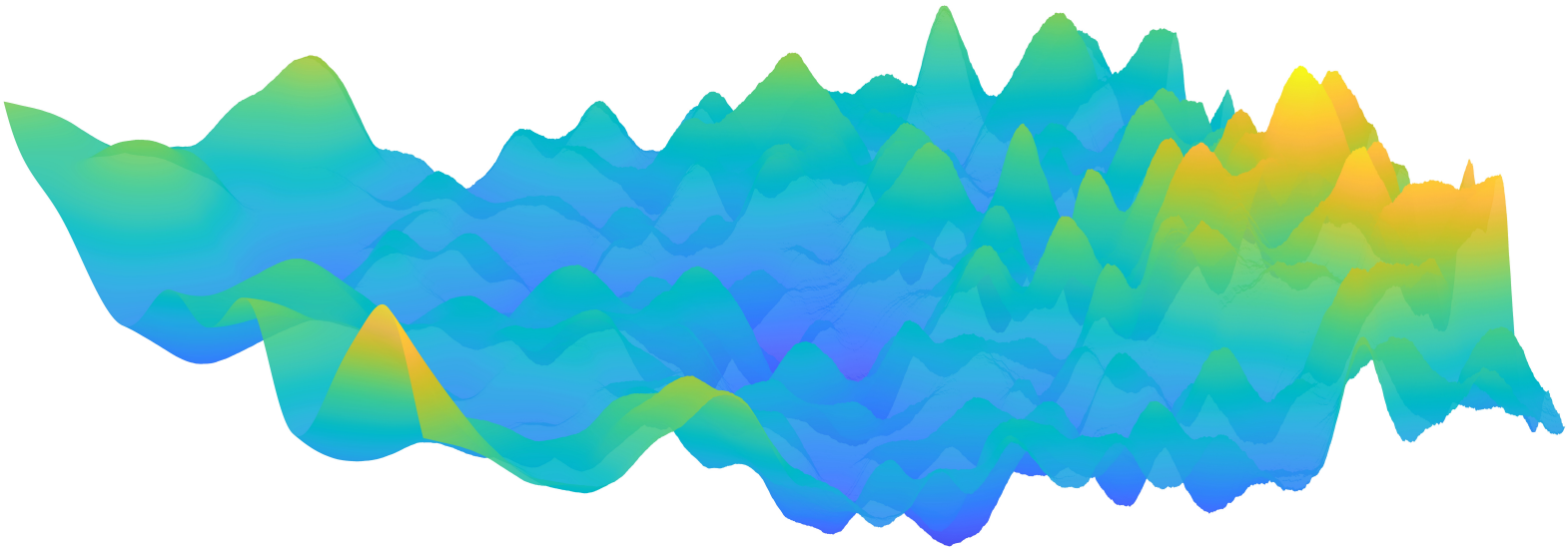

Supported by:

LGF UMR 5307 MATERIAUX, MECANIQUE, PROCEDES

GDR GeoSto

cnrs dépasser les frontières